Nanoscale Advances

Accepted Manuscript

This article can be cited before page numbers have been issued, to do this please use: A. D. Chowdhury, K. Takemura, I. M. Khorish, F. Nasrin, M. M. N. Tun, K. Morita and E. Y. Park, *Nanoscale Adv.*, 2020, DOI: 10.1039/C9NA00763F.

ROYAL SOCIETY OF CHEMISTRY

rsc.li/nanoscale-advances

View Article Online
DOI: 10.1039/C9NA00763F

Detection and identification of dengue virus serotype altering quantum dots and AuNP regulated localized surface plasmon resonance †

Ankan Dutta Chowdhury,[a] Kenshin Takemura,[b] Indra Memdi Khorish,[c] Fahmida Nasrin,[b] Mya Myat Ngwe Tun,[d] Kouichi Morita[d] and Enoch Y. Park[a,b,c,*]

[a] *Research Institute of Green Science and Technology, Shizuoka University, 836 Ohya Suruga-ku, Shizuoka 422-8529, Japan. E-mail: park.enoch@shizuoka.ac.jp*

[b] *Department of Bioscience, Graduate School of Science and Technology, Shizuoka University, 836 Ohya Suruga-ku, Shizuoka 422-8529, Japan.*

[c] *College of Agriculture, Graduate School of Integrated Science and Technology, Shizuoka University, 836 Ohya Suruga-ku, Shizuoka 422-8529, Japan.*

[d] *Department of Virology, Institute of Tropical Medicine, Nagasaki University, Sakamoto 1-12-4, Nagasaki City 852-8523, Japan.*

† Electronic supplementary information (ESI) available. See DOI:

View Article Online
DOI: 10.1039/C9NA00763F

Abstract:

Dengue hemorrhagic fever or dengue shock syndrome has become a severe human fatal disease caused by the infection with one of four closely related but serologically distinct Dengue viruses (DENVs). All four Dengue serotypes are currently co-circulating throughout the subtropics and tropics. As the fatality rate is increased severely when a secondary infection occurred by a virus serotype different from that of the initial infection, the serotype identification is equally important as the virus detection. In this study, the development and validation of a rapid and quantitative DENV serotype-specific (serotype 1–4) biosensor has been reported optimizing a stable system between Cadmium Selenide Telurium sulphide fluorescent quantum dots (CdSeTeS QDs) and gold nanoparticles (AuNPs). Four different nanoprobes are designed using each primer-probe serotype specific hairpin single stranded DNA, covalently bound at different position with CdSeTeS QDs which generates altered fluorescence signal for each serotype of DENV. In fourplex reactions with free functionalized AuNPs and four nanoprobes, standard dilutions of target virus DNA of 10^{-15} to 10^{-10} M were successfully detected. The limit of detection was found in the order of femtomolar in all four serotypes where the serotype detection ability was undoubtedly established. To confirm the applicability of this sensing performance in long chained complex RNA, the sensor was also applied successfully to the RNAs extracted from DENV culture fluids for serotype identification as well as quantification which can lead as a potential diagnostic probe for the point-of care detection.

View Article Online
DOI: 10.1039/C9NA00763F

Introduction

The Metallic nanoparticles like Au, Ag, Pt etc. influence the quantum yield of adjacent fluorophores in a manner dependent on the shape, sizes and concentration of the nanostructure.[1–3] Among these parameters, absorption and emission of the fluorescence materials and surface plasmon resonance wavelength of metal nanostructures, distance and spectral characteristics of nanoparticles play most important roles on the adjacent fluorophore's fluorescence.[4–7] If these all parameters are kept constant at their optimized condition, a fluorometric system can be established by modulating the distance between metal nanoparticles and quantum dots (QDs), based on their localized surface plasmon resonance (LSPR) effect. Recently, these types of systems have been emerged as useful alternatives for enhancing the sensitivity of different detection platforms in biosensing.[6, 8–11] The mechanism of plasmon enhancement or quenching can be mainly attributed to the shifting of excitation rate due to a local field effect from the adjacent metal nanoparticles and the shifted emission rate by surface plasmon coupled emission, which can control the fluorescence intensity.[2] The application of plasmonic metallic nanoparticles in biosensing has been stimulated by the interaction of these nanoparticles with electromagnetic waves, which induce oscillations of the plasmons (free electrons) at the particle surface.[1] This phenomenon has led to the development of LSPR-based biosensors for various analytes. To optimize the distance between these fluorescent QDs and metal nanoparticles, short chained oligomers can be used as a potential linker. Different surface plasmon resonance effect can be monitored on the QDs varying the length of the oligomers which can make a new system for the DNA/RNA detecting biosensor.

View Article Online
DOI: 10.1039/C9NA00763F

The development of ultrasensitive DNA/RNA detection is of great demand over this last decade for its various biomedical applications including gene profiling, drug diffusion, and clinical diagnostics.[12–17] Development of this DNA/RNA detection method in proper biosensing device has a great potential to gather maximum information from a small volume of analyte at very low cost. In case of viral disease detection, successful DNA/RNA based biosensors can offer significant advantages over existing diagnostic technologies like PCR, antigen-antibody interaction or protein identification in term of detection time and chances of reducing false positive responses.[18, 19] Recently, few fluorometric reports have claimed to achieve the desired low level detection.[20–22] However, most of the detection protocols are highly depended on the PCR amplification. This still remains as the most challenging task to overcome this limitation. In case of Dengue like viral fever, which affects a significant and ever-increasing portion of the world's population every year, the low detection level without any further application is in utmost need in respect to get a rapid detection tool. There are many reports can be found recently on Dengue DNA detection by RT-PCR, electrochemical and fluorometric methods[23–28] however successful application for point of-care detection without any amplification step including the ability of serotype identification from the clinically isolated RNA is rarely reported.

Herein, we report a new biosensing technique for the quantitative detection of DENV along with its serotype determination based on the distance dependent LSPR between CdSeTeS QDs and AuNPs. Firstly, four different nanoprobes are designed as hairpin structures where the loop portions of each hairpin are exactly complementary with the target analytes of four different DENV serotypes. The fixed regions of all hairpins are self-complementary by six poly guanine (poly-G) and poly cytosine (poly-C) where one side is

View Article Online
DOI: 10.1039/C9NA00763F

covalently bonded with the CdSeTeS QDs. In addition, an AuNPs functionalized with thiolated poly-C was also synthesized. In the sensing mixture of nanoprobes and the functionalized AuNPs, initially there should be no interaction between the AuNPs and the CdSeTeS QDs due to the closed hairpin structure of the single stranded probe DNA (ssDNA). However, after addition of complementary DNA/RNA of DENV, it can help to open the hairpin structure of the nanoprobe due to better hybridization of nanoprobe ssDNA and complementary RNA of DENV in its loop region and remains the poly-G region of nanoprobe free. Poly-C-functionalized AuNPs which are freely presented in the sensing solution can make complementary binding with the free poly-G region of the nanoprobe (as depicted in Fig. 1). The hairpin region has been designed as highly conserved sequence on the serotype of analyte DENV RNA. The distance between the QDs and the AuNPs should be situated by the base pairs of loop region at different position which triggers the LSPR enhancement (around 14 nm) or quenching (around 3 nm) effect on the fluorescence of QDs, depending on the distance. It is noteworthy that the extent of the LSPR-fluorescence signal changes is completely dependent on the concentration of the target analytes in the optimized condition for sensing, creating the calibration line in the range of concentration of 10^{-15} to 10^{-10} M.

Experimental

Materials

Phosphate saline buffer (PBS, pH 7.4), methanol, potassium hydroxide, polyoxyethyelene (20), sorbitan monolaurate (Tween 20), sulfuric acid, sodium citrate, tri-sodium citrate,

View Article Online
DOI: 10.1039/C9NA00763F

hydrogen peroxide, chloroform and acetone were purchased from FUJIFILM Wako Pure Chemical Ind. Ltd. (Osaka, Japan). Tetramethylbenzidine (TMBZ) was purchased from Dojindo (Kumamoto, Japan). $HAuCl_4$, *N*-(3-dimethylaminopropyl)-*N*-ethylcarbodiimide hydrochloride (EDC), bovine serum albumin (BSA), *N*-hydroxysuccinimide (NHS), 1-octadecene, tellurium (Te), L-cysteine, hexadecylamine (HDA), cadmium oxide (CdO), trioctylphosphine oxide (TOPO), trioctylphosphine (TOP), selenium (Se) and sulfur (S) were purchased from Sigma Aldrich (Saint Louis, MO, USA). Oleic acid was purchased from Nacalai Tesque (Kyoto, Japan).

Synthesis of CdSeTeS QDs

Synthesis of CdSeTeS QDs was carried out according to the previously reported method using organometallic hot-injection synthesis with CdO, Se, Te and S as the basic precursors.[29]

Synthesis of AuNPs

AuNP synthesis was carried out by citrate reduction method. In brief, 35 μL of 2 mM $HAuCl_4$ and 300 μL of 100 mM tri-sodium citrate were added into 25 mL of pure boiling water in a 100-mL flask under vigorous stirring condition. The solution was boiled for 15 min until the color changes to pink. Then the AuNP solution was cooled down at room temperature for further use.[30]

Preparation of oligomeric solutions and DENV RNAs from DENV culture fluids

View Article Online
DOI: 10.1039/C9NA00763F

A calculative amount of diethyl pyrocarbonate (DEPC) treated water, estimated by the supplier, was added to DNA containing well, purchased from FASMAC (Atsugi, Japan) to get the concentration of 1 mM as stock. Exact concentration of the DNA solutions was further verified by the absorption value at 260 nm in UV-Visible spectra.

Table 1. Following synthetic ssDNAs are used in this present work:

DNAs	Sequences
Probe DNA 1	NH_2-CCCCCC**CTTACCACCAGGGTACAGCTTCCCT**GGGGGGTTT
Probe DNA 2	CCCCCC**CCTTCCAGTGAGACTACAGCTTCAT**GGGGGGTTT-NH_2
Probe DNA 3	NH_2-CCCCCC**CTTTGCAAGGAGGTACAGCTTCCCT**GGGGGGTTT
Probe DNA 4	CCCCCC**CTTCCACCAGGAGTACAGCTTCCTC**GGGGGGTTT-NH_2
Probe DNA for AuNP	SH-AAAAAAAAA**AACCCCCC**T
Target DNAs	
ssDNA 1*	**AGGGAAGCTGTACCCTGGTGGTAAG**
ssDNA 2*	**ATGAAGCTGTAGTCTCACTGGAAGG**
ssDNA 3*	**AGGGAAGCTGTACCTCCTTGCAAAG**
ssDNA 4*	**GAGGAAGCTGTACTCCTGGTGGAAG**
Target DNAs for selectivity	
Influenza virus**	AAATACAACGGCATAATAACTGAAA[31]
Zika virus**	TGCTAAAACGCGGAGTAGCCCGTGT[32]
Norovirus**	TCCTGACATCATACAAGCTAACTCC[33]
Real samples	
Dengue RNAs	**Given in Table S1 ESI, the region has marked in green color.**

*These synthetic ssDNAs are synthesized according to the conserved region of Dengue RNAs as presented in the ESI, marked in green colour.

View Article Online
DOI: 10.1039/C9NA00763F

**For selectivity test, these synthetic ssDNAs are chosen from their corresponding references.

For the selectivity test, we have purchased synthetic DNAs from FASMAC (Atsugi, Japan) of influenza virus (A/California/7/2009) (H1N1),[31] zika virus[32] and genogroup II RNA of norovirus[33] according to the used DNAs mentioned in the references of their corresponding studies. In case of real sample analysis, DENV RNA was extracted from the DENV culture fluid using High Pure RNA Isolation kit (Roche Diagnostics, Mannheim, Germany) according to manufacturer's instructions. The virus strains used for this study were clinical isolates from dengue patients in the Philippines as follow: DENV-1, strain 99St12A; DENV-2, strain 00St22A; DENV-3, strain SLMC50; DENV-4, strain SLMC318.[34] These viruses were propagated onto C6/36 mosquito cell lines.

Functionalization of AuNPs with SH-AAAAAAAAAAACCCCCCT

The AuNPs solution was stirred for 2 h with 0.1 mM of thiol linked ssDNAs solution at pH 6.4 where the thiol group has been covalently linked with the AuNPs. After successful functionalization of the AuNPs, the nanocomposite was washed several times with DI water and centrifuged at 6000 × g to obtain oligonucleotide conjugated AuNPs free from excess probe ssDNA.

Preparation of nanoprobes

The synthesized CdSeTeS QDs were incubated with different hairpin-structured probe ssDNAs of 0.1 mM, corresponding to each DENV serotype via the covalent interaction

View Article Online
DOI: 10.1039/C9NA00763F

with the functionalized amine group of probe ssDNAs and the –COOH group of CdSeTeS QDs to construct the nanoprobe.[3] In brief, 3 mg of EDC is first mixed with 10 mg of carboxylic functionalized CdSeTeS QDs and then further activated with 5 mg of NHS for 30 min before addition of functionalized ssDNAs. The reaction mixture was then stirred overnight for the maximum conjugation of the probe ssDNA with the QDs and then purified by centrifugation (3000 × g) for 5 min. Resulting four kinds of hairpin-structured DENV 1–4 nanoprobes were obtained.

Physicochemical analysis

Transmission electron microscopy (TEM) images were obtained using TEM (JEM-2100F; JEOL, Tokyo, Japan) operated at 200 kV to check the size and surface morphology of the as synthesized nanocomposites. UV-Vis absorption and fluorescence spectra were obtained using a filter-based multimode microplate reader (Infinite® F500; TECAN, Ltd, Männedorf, Switzerland). X-ray diffraction (XRD) was carried out for all samples in dried powder form using a RINT ULTIMA XRD (Rigaku Co., Tokyo, Japan) with a Ni filter and a Cu-Kα source. Dynamic light scattering (DLS) measurements were performed using a Zetasizer Nano series (Malvern Inst. Ltd., Malvern, UK). Different chemical environment of CdSeTeS QDs nanocomposites before and after conjugation of AuNPs has been accounted thorough FTIR (ATR 8700, Shimadzu Co., Tokyo, Japan). The samples were dried in oven and then mixed homogenously with dried crystal of KBr to make the pellet. Then the pellet was immediately taken for the FTIR analysis to avoid any water absorption.

View Article Online
DOI: 10.1039/C9NA00763F

LSPR-mediated DENV serotype identification principle

Fig. 1 displays a pictorial overview of the preparation and detection principle of the biosensor. Firstly, the CdSeTeS QDs, conjugated with the hairpin ssDNAs were synthesized as mentioned above and then mixed with the functionalized AuNPs solution. There was no specific interaction occurred due to the close loop structure of the hairpin ssDNA in the nanoprobe. However, after addition of the target ssDNA/RNA sequences of each DENV serotypes, the target ssDNAs open up their complementary ssDNA loop sequence of the hairpin, forming a DNA/DNA or DNA/RNA hybridization. So, in this stage, a linear strand of the probe ssDNA conjugated with the QDs could be achieved where the target DNA/RNAs were aligned with the nanoprobe through the strong complementary binding. Initially, the synthetic ssDNA and probe ssDNAs were used for analysis. In the next case, the real RNA samples were used for sensing. Before addition of the target RNAs, the RNAs were heated up to 95 °C to denature any secondary structure between themselves and then added to the sensing solution immediately at room temperature. The probe ssDNAs concentration was always maintained at 1.1×10^{-9} M while the target ssDNAs concentrations were varied from 10^{-9} to 10^{-15} M. As a little excess amount of probe ssDNAs should not affect the fluorescence of the resulting solution (Fig. S1, ESI), we used little higher amount of the probe ssDNAs with respect to the target ssDNA of 100 µL. In addition, the Poly-C-functionalized AuNPs which were freely presented in the sensing solution also made complementary binding with the free poly-G region of the nanoprobe. Therefore, in all four cases of the DENV serotypes, the target DNA/RNAs made a linear structure of AuNP-complementary DNA/RNA-CdSeTeS QDs. Depending on the nanoprobe design, the QDs should be presented either in the far end or very close from the AuNP, as shown in the Fig. 1. As the enhancement or quenching of the

View Article Online
DOI: 10.1039/C9NA00763F

fluorescence signal were triggered based on the distance between the QDs and the bonded plasmonic AuNPs, different change of signal can be obtained on different analyte. The extent of the fluorescence enhancement/quenching of the QDs was dependent on the LSPR signal from AuNPs which was equivalent to the concentration of the target DNA/RNA.

Results and discussion

Characterizations of CdSeTeS QD-dsDNA-AuNP nanocomposites

TEM image of as synthesized AuNPs is observed in Fig. 2A where the spherical particle shape is consistently obtained with homogeneous distribution. The distribution has been calculated in Fig. 2B in the range of 30 – 50 nm with the average particle size of 39 ± 0.5 nm. As the particle size of the SPR molecule can influence the LSPR intensity largely, the homogeneity of the AuNP is highly desired. Similarly, the as synthesized CdSeTeS QDs are also analyzed in TEM, distributed in the range of 7 – 15 nm with the average particle size of 11.4 ± 0.5 nm (Fig. 2C). The UV-Vis spectrum of the CdSeTeS QDs is given in Fig. S2 of ESI, showing the signature absorption hump of CdSeTeS QDs at 540 nm which indicates its successful synthesis.[29, 35] After successful conjugation of the nanocomposites through the analytes ssDNA, CdSeTeS QD-dsDNA-AuNP was further characterized by TEM. For the characterization purpose, the DENV 1 target analyte has been used to construct the CdSeTeS QD-dsDNA-AuNP nanocomposites. As the other 3 target ssDNAs have the similar structure with DENV 1 and form the identical nanocomposite conformation, all the characterizations have been carried out for CdSeTeS QD-dsDNA-AuNP nanocomposites with DENV 1. In Fig. 2E, it is clearly observed from the image that

View Article Online
DOI: 10.1039/C9NA00763F

the small sized QDs (~5.9 nm) (Fig. 2D) and the AuNP (~40 nm) were closely arranged due to the covalent attachment controlled by the short linker of ssDNA chain. The concentration of the AuNP was given in much less than the CdSeTeS QDs concentration, hence the relatively high amounts of QD were found near each single AuNP (Fig. 2E). The nanocomposites formation was further verified by hydrodynamic diameter measurement where the CdSeTeS QD-dsDNA-AuNP nanocomposites along with its individual components were determined by DLS (Fig. 2F). The bare CdSeTeS QDs and AuNPs shows the hydrodynamic size of 7.5 ± 0.5 nm and 27.4 ± 1.5 nm, respectively which is little altered than its solid-state size, calculated from the TEM image. Being small sized and charged particles, the QDs and the AuNP are well solvated in aqueous buffer medium, resulting decrease of their hydrodynamic radius.[36] In case of CdSeTeS QD-dsDNA-AuNP nanocomposites, it shows the diameter of 76 ± 2.8 nm which is larger than their individual sizes, confirming the agglomerated distribution, which was also corroborated by TEM image. In case of elemental mapping of an isolated cluster of CdSeTeS QD-dsDNA-AuNPs nanocomposite as depicted in Fig. 2G, the individual elements have been observed distinctly. The nanocomposite was mapped with Au and Cd as shown in Fig. $2G_i$ and $2G_{ii}$, respectively whereas their merged image in Fig. $2G_{iii}$ has proved about the successful linkage of these two components of CdSeTeS QDs and AuNP by the ssDNA chain.

The nanocomposite was further characterized by XRD spectra to illustrate the structural changes of two crystalline components of CdSeTeS QDs and AuNPs. The crystalline nature of the bare AuNPs was confirmed by the XRD analysis. In Fig. 3A, the diffraction features of bare AuNP shows two characteristic peaks at 38.1° and 44.6° corresponding to the (111) and (200) planes, respectively.[37] Similarly, the diffraction

View Article Online
DOI: 10.1039/C9NA00763F

pattern of the bare CdSeTeS QDs indicates that the QDs are highly crystalline and cubic in nature (Fig. 3A), exhibiting three characteristic peaks at 2 theta of 26.7°, 44.2° and 51.8° for (111), (220) and (311) crystal planes respectively.[33] It is noteworthy that the position of these peaks remains almost unchanged even after conjugation with AuNPs, indicating that the attachment only takes place in the functional groups of the CdSeTeS QDs without affecting its own crystal lattice. In addition, two small but clear peaks at 2theta = 38.1° and 44.6° have been introduced in the spectra due to the incorporation of the AuNPs on the nanocomposites, confirming the successful formation of the CdSeTeS QD-dsDNA-AuNPs. However, the relative intensities of the Au peaks have become less intense obviously and partially overlapped at 44.6° by the 44.2° peak of CdSeTeS QDs as the contribution of AuNPs is much lower than the CdSeTeS QDs in the CdSeTeS QD-dsDNA-AuNPs nanocomposites. Therefore, it can be concluded from the XRD results that the structural conformation of the AuNPs and QDs remain same even after the nanocomposite formation. Therefore, any changes of fluorescence came from the nanocomposites are solely depended on the LSPR effect.

FTIR spectroscopy analysis was also carried out to reveal the conjugation of DNA with the AuNP and its subsequent binding to CdSeTeS QDs in Fig. 3B. In case of the bare CdSeTeS QDs, the spectrum appeared with all of its standard transmitted peaks as reported earlier, particularly at its 1735 cm^{-1} peak assigned as the asymmetric carboxylate ($–COO^–$) group.[33] In case of bare AuNP, the FTIR spectra has revealed the presence of different functional groups such as hydroxyl, amine and –COOH linkages. In case of the CdSeTeS QD-dsDNA-AuNPs nanocomposites, the bands are observed at 3410.1 cm^{-1}, 2953.3 cm^{-1} and 1735.6 cm^{-1}, acknowledged as $–OH/NH_2$ stretching, C–H stretching, and C–O

View Article Online
DOI: 10.1039/C9NA00763F

stretching of carboxylic acid, respectively.[38] The band at 1160 cm^{-1} represents the C–N stretching which is quite common for DNA, indicating the presence of DNA in AuNPs.[39] The band at 1059 cm^{-1} are the characteristic peak, assigned to the vibration of ribose (C-C sugar) or associated with the phosphate groups of DNA.[40] Another indicative peak also has been noticed at 839 cm^{-1} for the antisymmetric vibration of P-O bond of phosphate group (839 cm^{-1}) of DNA.[41] The combination of these characteristic peaks of the nanocomposites with DNA indicates the successful formation of the AuNP-DNA with the CdSeTeS QDs.

Designing four DENV nanoprobes for serotype detection employing the distance dependent LSPR mechanism

LSPR that comes from the surface resonance electrons of the noble metal nanoparticles like Au, Ag etc. can have either enhancement or quenching effects on the adjacent fluorophore. It depends on the distance of the fluorophores separated from the metal nanoparticle and its relative position of the LSPR wavelength from the excitation or emission wavelength of the fluorophores.[5] The fluorescence property of the CDSeTeS QDs has measured by calculating its quantum efficiency (quantum yield = 0.33, given in Fig. S3, ESI) which is quite satisfactory for this fluorometric investigation. Therefore, the quantum efficiency and the emission intensity of the fluorophores, CdSeTeS QDs can be enhanced or quenched by their surrounding metal nanoparticles of AuNP by the equilibrium of two-way of electron transfer process of non-radiative energy transfer and local field enhancement effect.[2] When these two duos are in very close proximity (for example ~2 nm), non-radiative energy transfer dominates, which results the quenching of the fluorescence. Due to the increased distance, the local field enhancement effect becomes significant, contributing to the

View Article Online
DOI: 10.1039/C9NA00763F

enhancement of fluorescence intensity. The emission intensity reaches maximum at an optimal distance of about 14 – 20 nm depending on the size and shape of both nanocomponents as depicted in the schematic diagram of Fig. 4A. When the distance is increased to more than 20 nm, the fluorescence intensity does not have any significant effect of the neighboring group of metal nanoparticles. Therefore, in case of large distance from the AuNPs, electric field intensity becomes insignificant, causing no observable changes in the emission intensity of CdSeTeS QDs.

Employing the distance dependent fluorescence behavior, we have designed four types of nanoprobes for four specific DENV serotypes. As illustrated in Fig. 4B, four hairpin structures with 40 bp ssDNA oligonucleotides were synthesized, consisted of 5′ / 3′ terminus with an amino group (NH_2) for the CdSeTeS QDs conjugation. The probes contained 25 bp complementary sequences with four DENV serotypes assigned in four different colors in the scheme in Fig. 4B. The remaining 15 bp were designed with 6 poly-G and 6 poly-C for the loop formation in addition with 3 bp T in poly-C end. Therefore, after conjugation with their complementary DENV serotype ssDNA, the loop can be opened up and the GGGGGGTTT region can be bonded with the free AuNP-SH-CCCCCCAAAAAAAAAAAA probe, presented free in the sensing solution. The probe ssDNA has 6 G-C complementary binding whereas 25 unbound nucleotides in loop region. After addition of the target ssDNAs, the conjugated structure contained 25 complementary bonded nucleotides with target ssDNA and 6 new G-C binding with free AuNPs with 6 free nucleotides in the end which indicates the higher stability of the conjugated structure over the former. Additionally, with compared with similar studies on DNA hairpin, it can be concluded that the straight chain formation of the DNA has much higher stability than the looped one due to

View Article Online
DOI: 10.1039/C9NA00763F

much higher number of complementary DNA nucleotides.[42–44] As the NH_2 group is bonded with the ssDNA nanoprobes in 5′ end in the case of DENVs 2 and 4, CdSeTeS QDs should be positioned very close to the AuNP (< 6 nm), expecting quenching. On the other hand, in the case of DENVs 1 and 3, as the NH_2 group is bonded with the ssDNA nanoprobes in 3′ end, the distance between the AuNP and the CdSeTeS QDs should be formed at a distance of approx. 40 bp or 12 14 nm, expecting fluorescence enhancement. The initial fluorescence of the probe showed only the fluorescence of the QDs as designated in the scheme of Fig. 1A. However, the QD fluorescence increased in presence of AuNP when situated in a certain distance between the QD and the AuNP due to the LSPR effect. Therefore, after addition of the DENV 1/3, the target ssDNA bound the loop structure of the probe ssDNA and opened it, in such way that the distance between the QD and the AuNP are in ~14 nm which is perfect for the LSPR effect, hence resulting enhancement of the QD fluorescence from its initial value as depicted in Fig. 1B. These two types of conjugation are shown in Fig. 4C, where the DENV 1 enhances the fluorescence of CdSeTeS QDs whereas the DENV 2 produces the quenching effect as compared to the bare CdSeTeS QDs, supporting our hypothesis of this present work.

DENV serotype detection

The nanoprobes of four types of ssDNA-CdSeTeS QDs and ssDNA-AuNPs were mixed with 4 serotypes of DENV ssDNAs (DENV-1, 2, 3 and 4), separately for the serotyping. From different vials, we can get four different positioned CdSeTeS QD-DNA-AuNP nanocomposites where the distance between AuNPs and the CdSeTeS QDs are also different. The fluorescence intensity was recorded at the wavelength range of 500 – 700 nm at the excitation of the CdSeTeS QDs at 480 nm. It is clear from the Figs. 5A–D, the

View Article Online
DOI: 10.1039/C9NA00763F

nanocomposites show their respective fluorescence enhancement for DENVs 1 and 3 (Figs. 5A, C) and quenching for DENVs 2 and 4 (Figs. 5B, D). To check their cross reactivity, the interaction between all sixteen possible combination of the four nanoprobes with four serotype target DENV ssDNAs were presented in Fig. 5E and their schematic representation are shown in the diagram of Fig. 5F. It is clearly observed that the assigned nanoprobes which are designed for the specific DENV analyte, are very much sensitive for the exact complementary target ssDNAs where the other ssDNAs and the bare buffer medium show almost insignificant signals. In case of DProbe 1, the target DENV 1 shows the change of fluorescence of 17.1 % with respect to the initial fluorescence whereas the DENV 2, 3 and 4 shows only the 2.3, −1.4 and −1.6 % of changes which are almost ignorable compared with the target signals. Similar or better specificity were observed in case of other probes of DProbe 2, DProbe 3 and DProbe 4. Therefore, from these above results, we can get the exact information about the DENV serotype. By changing the QDs with different emission wavelength in future, we can also distinguish the exact serotype in one pot reaction mixture.

Calibration for four DENV serotypes

After successful identification of serotype, the quantification of the target ssDNA is examined and expressed in term of their corresponding calibration lines in Fig. 6. Fluorescence spectra depending on four target analytes are given in Fig. 6A – D which are representing four serotypes of DENV ssDNAs in the concentration range of 10^{-15} to 10^{-9} M with their individually designed CdSeTeS QD-dsDNA-AuNP nanoprobes. A steady increase in the fluorescence intensity was achieved in case of DENVs 1 and 3 (Fig. 6A and C) whereas the decreases of peak intensities were observed in case of DENVs 2 and 4 (Fig.

View Article Online
DOI: 10.1039/C9NA00763F

6B and D). The calibration lines from these four graphs are plotted in Fig. 6E where the linear calibration lines have been found for all in the concentration range from 10^{-15} to 10^{-10} M. In case of 10^{-9} M concentration or above, signals tend to their saturation. The correlation coefficients are found in the range of 0.978 to 0.99. The quenching calibration lines for DENVs 2 and 4 are maintained equal slope however the enhanced calibrations for DENVs 1 and 3 changes greatly. Due to small difference in guanidine bases content for all serotypes' duplexes, the exact formation of CdSeTeS QD-dsDNA-AuNP with analyte ssDNA may be not exactly the same. As the distance is very much sensitive for the LSPR enhancement, the concentration vs. fluorescence signals are slightly varied from each other, producing different slopes. In addition, the probe ssDNA for DENV 1 forms different type of hairpin structure with higher energy of 7 kcal/mol compared to others three of 4.9–5.1 kcal/mol. The most possible secondary structures of all four ssDNA probes are given in Fig. S4, ESI. Therefore, due to the more conjugated hairpin, the slope of the enhanced intensity for DENV 1 shows lower than the DENV 3. The limit of detection (LOD) was calculated by 3 × standard deviation of lowest signal divided by slope of the calibration line[45] and found 24.6, 11.4, 39.8 and 39.7 fM for DENVs 1, 2, 3 and 4 with the correlation coefficient (R^2) of 0.964, 0.963, 0.995 and 0.972, respectively.

Detection of four DENV serotypes isolated from real sample with the proposed sensor

After successful detection of the synthetic small target ssDNAs, the sensing application has been extended towards the real DENV samples. The aim of this present work is to apply the protocol in the direct extracted DENV RNAs without any further pre-treatment or amplification process. DENV RNAs were extracted from four serotypes of DENV culture

View Article Online
DOI: 10.1039/C9NA00763F

fluids and the four types of nanoprobes then treated for the analysis. The sequences of the full RNAs are given in the Table S1, ESI. To avoid any secondary loop formation of the RNAs, the RNA samples were incubated at 95 °C for 2 min before analysis. During the cooling time to the normal temperature, the sensor was added to the RNA samples which helped to make stronger hybridization between the loop region of nanoprobe with the RNA strand. The stability of the RNAs at 95 °C are also measured in the UV-Vis spectra, as presented in Fig. S5, ESI. As presented in Fig. 7A, the fluorescence signal of CdSeTeS QDs has been clearly altered depending on the analyte serotype, similar as those of the synthetic ssDNAs in Fig. 5E. The fluorescence curves are given in Fig. S6, ESI for all four samples, reacted with all four nanoprobes and their comparative bar diagram has calculated in Fig. 7A. The percentage changes are not as good as the previous calibration line in DI water. Particularly in case of DProbe3, the change of fluorescence is 19.2 % for DENV 3 with respect to the initial fluorescence whereas the DENV 1, 2 and 4 shows 2.9, 3.1 and 4.6 % respectively. However, considering the presence of other interferences in the sample medium, this 4-fold enhancement can be acceptable for the real analysis where the concentration of the RNA is in picomolar range. In case of DProbe 1, 2 and 4, changes are 23.7, −13.4 and −12.9 % for their corresponding targets where the signals for other interferences are almost negligible. The sensor was then tested for the detection of the RNA samples where the concentration was diluted in four separate solutions to make the proper calibration lines. The percentage changes of the obtained fluorescence for each serotype have been plotted in the Fig. 7B and their corresponding calibration lines are generated. The calibration lines for the real RNA analysis has plotted in bold black lines which are compared with the calibration lines found in water medium. The 5, 10, 50 and 100-fold diluted results maintain the linearity for all

View Article Online
DOI: 10.1039/C9NA00763F

serotypes. Although the slopes of the calibration lines are deviated largely from the water medium, however, they are still following the linearity. Here, the probe to target binding is DNA/RNA instead of DNA/DNA which may be the reason for the decrease of the slope. It is obvious that the binding nature of RNA/RNA and RNA/DNA is not exactly the same,[46] however, to understand the trend of binding for the sensing application in this work, the comparison of these two calibration lines are quite satisfactory. All the nanoprobes are also tested with the bare medium and found that the nanoprobes still show the desired sensitivity for the exact complementary targets even in the complex medium. To confirm the applicability in real sample analysis, evaluating in different isolates representing different lineages of each serotype should be also required. In future, before proceeding to the on-site monitoring, detectability in different lineage of each serotype need to be established. In addition, few other viral synthetic ssDNAs had also used with the sensor to check any possible non-specific interaction. Zika virus is chosen as it is from same flavivirus family of Dengue whereas Influenza is a mostly common enveloped virus like Dengue. The Norovirus has been selected as an example of non-enveloped virus. The nanoprobes showed negligible interactions with Zika virus and Norovirus, as presented in Fig. S7, ESI, confirming the absence of any non-specific interaction from any part of the nanoprobe. In case of Influenza virus, there are 1.37-fold enhancement noticed compared with the sensor whereas the target virus of DENV 1 shows 3.64-fold of enhancement which is quite high to confirm its specific nature. Therefore, from these above results, it can be concluded that the CdSeTeS-dsDNA nanoprobes can successfully identify the DENV serotypes with the detection of the analyte concentration in DENV culture fluid samples which can serve as an alternative for point-of-care diagnosis in serotype determination of DENV.

View Article Online
DOI: 10.1039/C9NA00763F

Conclusions

A sensitive DENV DNA detection biosensor with the serotype identification ability was proposed in the present study by altering the distance-based LSPR between AuNPs and CdSeTeS QDs. Four different nanoprobes were constructed using each primer-probe serotype specific hairpin ssDNAs with CdSeTeS QDs by covalent bond. The synthesized nanoprobes can successfully identify the DENV serotypes where the fluorescence enhancement represents for DENVs 1 and 3 and quenching indicates the presence of DENVs 2 and 4. In reaction with free ssDNA functionalized AuNPs and nanoprobes, target ssDNA of 10^{-15} to 10^{-10} M were successfully detected. The limit of detection was calculated as 24.6, 11.4, 39.8 and 39.7 fM for the synthetic ssDNAs of DENVs 1, 2, 3 and 4, respectively. To the best of our knowledge, this is the first attempt on the DENV serotype detection along with quantification without any amplification employing the distance dependent LSPR phenomenon of fluorescent CdSeTeS QDs with its adjacent AuNPs. In addition, to confirm its applicability in complex system, the sensor was also applied to the real DENV RNAs extracted from DENV culture fluids without pre-treatment and showed satisfactory performances for serotype identification with quantification. This result can lead the sensing process as a potential diagnostic probe for the point-of care detection in future.

Conflicts of interest

There are no conflicts to declare.

Acknowledgements

View Article Online
DOI: 10.1039/C9NA00763F

ADC thanks the Japan Society for the Promotion of Science (JSPS) for a postdoctoral fellowship (No. P17359). This work was supported and partly by the Bilateral Joint Research Project of the JSPS, Japan.

References

1. L. Zhang, Y. Song, T. Fujita, Y. Zhang, M. Chen and T. H. Wang, *Adv. Mat.*, 2014, **26**, 1289–1294.
2. A. L. Feng, M. L. You, L. Tian, S. Singamaneni, M. Liu, Z. Duan, T. J. Lu, F. Xu and M. Lin, *Sci Rep*, 2015, **5**, 7779.
3. F. Nasrin, A. D. Chowdhury, K. Takemura, J. Lee, O. Adegoke, V. K. Deo, F. Abe, T. Suzuki and E. Y. Park, *Biosen. Bioelectrons.*, 2018, **122**, 16–24.
4. M. Li, S. K. Cushing, Q. Wang, X. Shi, L. A. Hornak, Z. Hong and N. Wu, *J. Phys. Chem. Lett.*, 2011, **2**, 2125–2129.
5. M.-X. Li, W. Zhao, G.-S. Qian, Q.-M. Feng, J.-J. Xu and H.-Y. Chen, *Chem. Commun.*, 2016, **52**, 14230–14233.
6. K. Takemura, O. Adegoke, N. Takahashi, T. Kato, T.-C. Li, N. Kitamoto, T. Tanaka, T. Suzuki and E. Y. Park, *Biosen. Bioelectrons.*, 2017, **89**, 998–1005.
7. Y. Ke, X. Wen, D. Zhao, R. Che, Q. Xiong and Y. Long, *ACS Nano*, 2017, **11**, 7542–7551.
8. A. Neely, C. Perry, B. Varisli, A. K. Singh, T. Arbneshi, D. Senapati, J. R. Kalluri and P. C. Ray, *ACS Nano*, 2009, **3**, 2834–2840.
9. J. Wang, Y. Shan, W.-W. Zhao, J.-J. Xu and H.-Y. Chen, *Anal. Chem.*, 2011, **83**, 4004–4011.
10. C. Li, C. Wu, J. Zheng, J. Lai, C. Zhang and Y. Zhao, *Langmuir*, 2010, **26**, 9130–9135.

View Article Online
DOI: 10.1039/C9NA00763F

11. H. Nishi, S. Hiroya and T. Tatsuma, *ACS Nano*, 2015, **9**, 6214–6221.

12. X. Zhao, R. Tapec-Dytioco and W. Tan, *J. Am. Chem. Soc.*, 2003, **125**, 11474–11475.

13. A. H. Loo, Z. Sofer, D. Bouša, P. Ulbrich, A. Bonanni and M. Pumera, *ACS Appl. Mater. Interfaces*, 2016, **8**, 1951–1957.

14. J.-L. Ma, B.-C. Yin, H.-N. Le and B.-C. Ye, *ACS Appl. Mater. Interfaces*, 2015, **7**, 12856–12863.

15. A. D. Chowdhury, R. Gangopadhyay and A. De, *Sensors Actuators B: Chem.*, 2014, **190**, 348–356.

16. A. Dutta Chowdhury, N. Agnihotri, R.-a. Doong and A. De, *Anal Chem*, 2017, **89**, 12244–12251.

17. S. Dutta, A. D. Chowdhury, S. Biswas, E. Y. Park, N. Agnihotri, A. De and S. De, *Biochem. Eng. J.*, 2018, **140**, 130–139.

18. J. Lee, M. Morita, K. Takemura and E. Y. Park, *Biosens. Bioelectron.*, 2018, **102**, 425–431.

19. E. Nebling, T. Grunwald, J. Albers, P. Schäfer and R. Hintsche, *Anal. Chem.*, 2004, **76**, 689–696.

20. X. Lu, X. Dong, K. Zhang, X. Han, X. Fang and Y. Zhang, *Analyst*, 2013, **138**, 642–650.

21. Y. Zhang, C. Zhu, L. Zhang, C. Tan, J. Yang, B. Chen, L. Wang and H. Zhang, *Small*, 2015, **11**, 1385–1389.

22. M. Stanisavljevic, S. Krizkova, M. Vaculovicova, R. Kizek and V. Adam, *Biosens. Bioelectron.*, 2015, **74**, 562–574.

23. A. Dutta Chowdhury, A. B. Ganganboina, F. Nasrin, K. Takemura, R.-a. Doong, D. I. S. Utomo, J. Lee, I. M. Khoris and E. Y. Park, *Anal Chem*, 2018, **90**, 12464–12474.

View Article Online
DOI: 10.1039/C9NA00763F

24. M. N. MN, U. Hashim, M. M. Arshad, S. Kasjoo, S. Rahman, A. Ruslinda, M. Fathil, R. Adzhri and M. Shahimin, *Biosens. Bioelectron.*, 2016, **83**, 106–114.

25. M. A. Iyer, G. Oza, S. Velumani, A. Maldonado, J. Romero, M. d. L. Munoz, M. Sridharan, R. Asomoza and J. Yi, *Sensors Actuators B: Chem.*, 2014, **202**, 1338–1348.

26. A. A. Odeh, Y. Al-Douri, C. Voon, R. M. Ayub, S. C. Gopinath, R. A. Odeh, M. Ameri and A. Bouhemadou, *Microchim. Acta*, 2017, **184**, 2211–2218.

27. N. Mehta, B. Perrais, K. Martin, A. Kumar, T. C. Hobman, M. N. Cabalfin-Chua, M. E. Donaldo, M. S. S. Painaga, J. Y. Gaite and V. Tran, *Am J Trop Med Hyg*, 2019, **100**, 1534–1540.

28. E. M. Euliano, A. N. Hardcastle, C. M. Victoriano, W. E. Gabella, F. R. Haselton and N. M. Adams, *Sci Rep*, 2019, **9**, 1–11.

29. O. Adegoke, T. Nyokong and P. B. Forbes, *J Alloys Comp*, 2015, **645**, 443–449.

30. S. V. Salihov, Y. A. Ivanenkov, S. P. Krechetov, M. S. Veselov, N. V. Sviridenkova, A. G. Savchenko, N. L. Klyachko, Y. I. Golovin, N. V. Chufarova and E. K. Beloglazkina, *J. Magn. Magn. Mater.*, 2015, **394**, 173–178.

31. O. Adegoke, T. Kato and E. Y. Park, *Biosen. Bioelectrons.*, 2016, **80**, 483–490.

32. O. Adegoke, M. Morita, T. Kato, M. Ito, T. Suzuki and E. Y. Park, *Biosen. Bioelectrons.*, 2017, **94**, 513–522.

33. O. Adegoke, M.-W. Seo, T. Kato, S. Kawahito and E. Y. Park, *Biosen. Bioelectrons.*, 2016, **86**, 135–142.

34. M. H. P. Ly, M. L. Moi, T. B. H. Vu, M. M. N. Tun, T. Saunders, C. N. Nguyen, A. K. T. Nguyen, H. M. Nguyen, T. H. Dao and D. Q. Pham, *BMC infectious diseases*, 2018, **18**, 31.

View Article Online
DOI: 10.1039/C9NA00763F

35. G.-C. Fan, H. Zhu, Q. Shen, L. Han, M. Zhao, J.-R. Zhang and J.-J. Zhu, *Chem. Commun.*, 2015, **51**, 7023–7026.

36. C. Zhang, X. Li, C. Tian, G. Yu, Y. Li, W. Jiang and C. Mao, *ACS Nano*, 2014, **8**, 1130–1135.

37. S. Krishnamurthy, A. Esterle, N. C. Sharma and S. V. Sahi, *Nanoscale Res. Lett.*, 2014, **9**, 627.

38. G.-X. Liang, M.-M. Gu, J.-R. Zhang and J.-J. Zhu, *Nanotechnology*, 2009, **20**, 415103.

39. S. M. Watson, H. D. A. Mohamed, B. R. Horrocks and A. Houlton, *Nanoscale*, 2013, **5**, 5349–5359.

40. S. R. Ede, A. Ramadoss, S. Anantharaj, U. Nithiyanantham and S. Kundu, *Phys Chem Chem Phys*, 2014, **16**, 21846–21859.

41. A. C. Moço, P. H. Guedes, J. M. Flauzino, H. S. da Silva, J. G. Vieira, A. C. Castro, É. V. Gomes, F. M. Tolentino, M. M. Soares and J. M. Madurro, *Electroanalysis*, 2019, **31**, 1580–1587.

42. P. Zhang, T. Beck and W. Tan, *Angew Chem*, 2001, **40**, 402–405.

43. F. Li, Y. Huang, Q. Yang, Z. Zhong, D. Li, L. Wang, S. Song and C. Fan, *Nanoscale*, 2010, **2**, 1021–1026.

44. S. Deng, L. Cheng, J. Lei, Y. Cheng, Y. Huang and H. Ju, *Nanoscale*, 2013, **5**, 5435–5441.

45. A. D. Chowdhury, N. Agnihotri, A. De and M. Sarkar, *Sensors Actuators B: Chem.*, 2014, **202**, 917–923.

46. F. A. Tanious, J. M. Veal, H. Buczak, L. S. Ratmeyer and W. D. Wilson, *Biochemistry*, 1992, **31**, 3103–3112.

View Article Online
DOI: 10.1039/C9NA00763F

Legends for figures

Fig. 1 Schematic representation for the detection mechanism of DENV by AuNP and hairpin ssDNA-CdSeTeS QDs: (A) Probe design for DProbe 1 and 2 and functionalized AuNP, (B) Identification and fluorometric enhancement for DENV 1/3 serotype and quenching for DENV 2/4 serotype depending on the distance between the nanocomposite of AuNP-dsDNA-CdSeTeS.

Fig. 2 TEM images and size distributions of AuNPs (A & B) and CdSeTeS QDs (C & D), (E) TEM image of CdSeTeS QDs-dsDNA-AuNPs, (F) DLS for hydrodynamic sizes of CdSeTeS QDs, AuNP and CdSeTeS QDs-dsDNA-AuNP nanocomposites, (G) STEM mapping of CdSeTeS QDs-dsDNA-AuNP, (Gi) Au, (Gii) Cd and (Giii) merged image.

Fig. 3 Characterizations of AuNP, CdSeTeS QDs and CdSeTeS-dsDNA-AuNP nanocomposites in XRD (A) and FTIR (B).

Fig. 4 (A) Schematic representation of distance based LSPR effect of AuNP on CdSeTeS QDs, (B) schematic representation for preparing of 4 types of hairpin probe for sensing, (C) Fluorescence properties of CdSeTeS QDs, and CdSeTeS QDs-dsDNA-AuNP nanocomposites with DENV 1 and DENV 2.

Fig. 5 Distance dependent fluorescence intensities changes of CdSeTeS QDs of four different sensing nanoprobe in presence of four different analytes of DENV 1 (A), DENV 2 (B), DENV 3 (C) and DENV 4 (D) serotypes. (E) Comparative bar diagram for the cross sensitivity of all four nanoprobes in presence of all four types of DENV serotypes, (F) Pictorial illustration for the cross-reactivity determination of the sensor.

View Article Online
DOI: 10.1039/C9NA00763F

Fig. 6 (A–D) Concentration dependent fluorescence changes of CdSeTeS-dsDNA-AuNP nanocomposites in presence of target analyte DENV ssDNA of all four serotypes in the concentration range of 10^{-15} to 10^{-9} M, (E) Calibration curves for all four DENV serotypes.

Fig. 7 (A) Comparative analysis of all four nanoprobes in presence of all four types of DENV RNA serotypes, (B) Quantification of the Dengue RNA isolated from DENV culture fluid: Intensities found from the fluorescence of each sample; ◆Dengue 1, ◆Dengue 2, ◆Dengue 3 and ◆Dengue 4, quantified from their calibration lines found from the buffer solution. The black calibration lines are plotted from the RNA concentration.

View Article Online
DOI: 10.1039/C9NA00763F

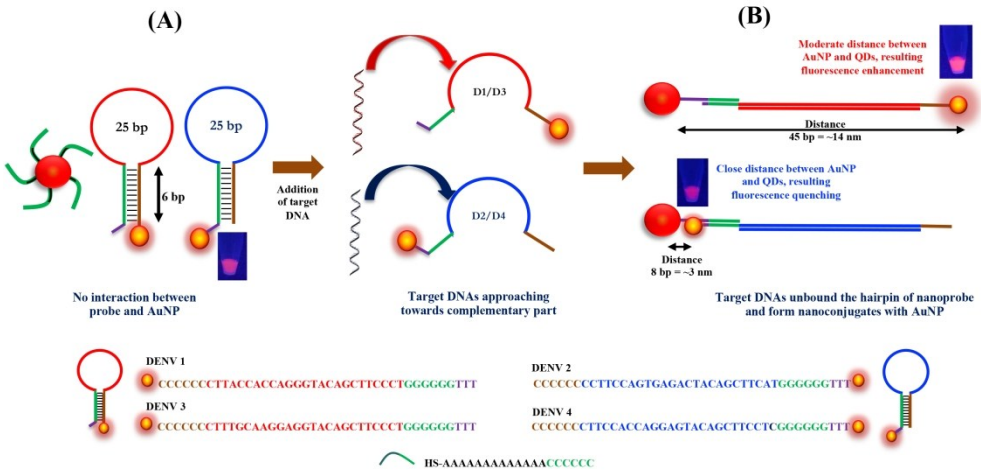

Fig. 1

View Article Online
DOI: 10.1039/C9NA00763F

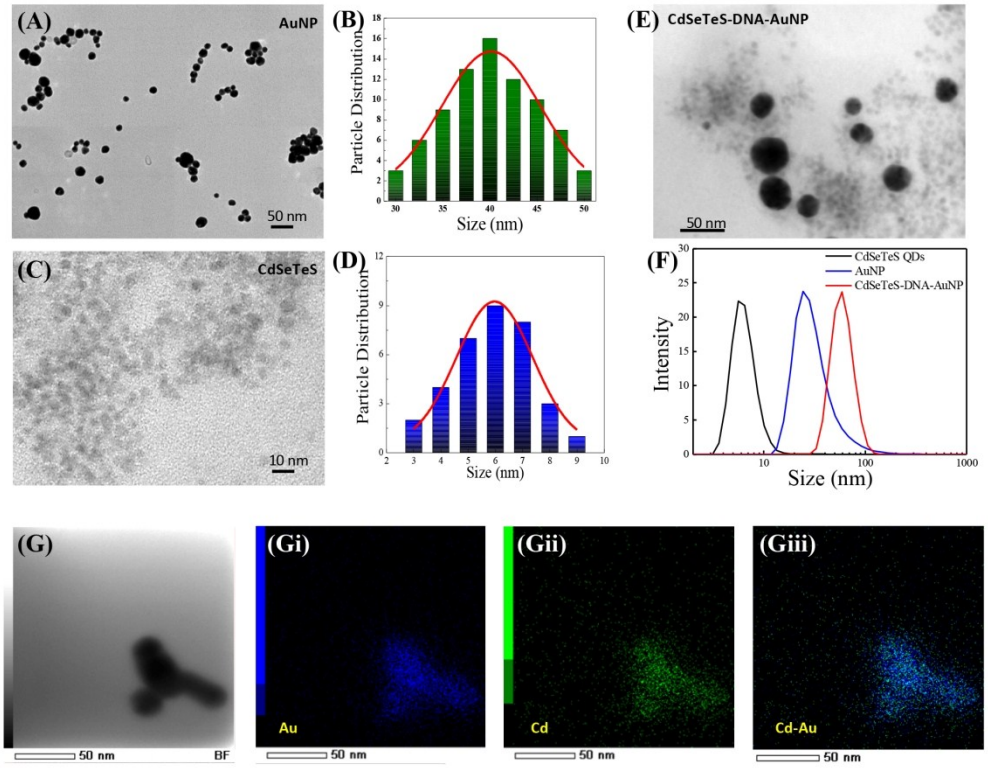

Fig. 2

View Article Online
DOI: 10.1039/C9NA00763F

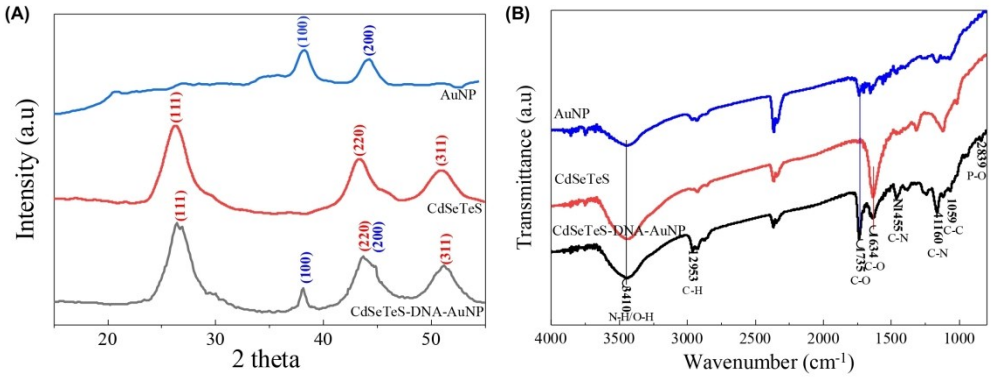

Fig. 3

233x89mm (300 x 300 DPI)

View Article Online
DOI: 10.1039/C9NA00763F

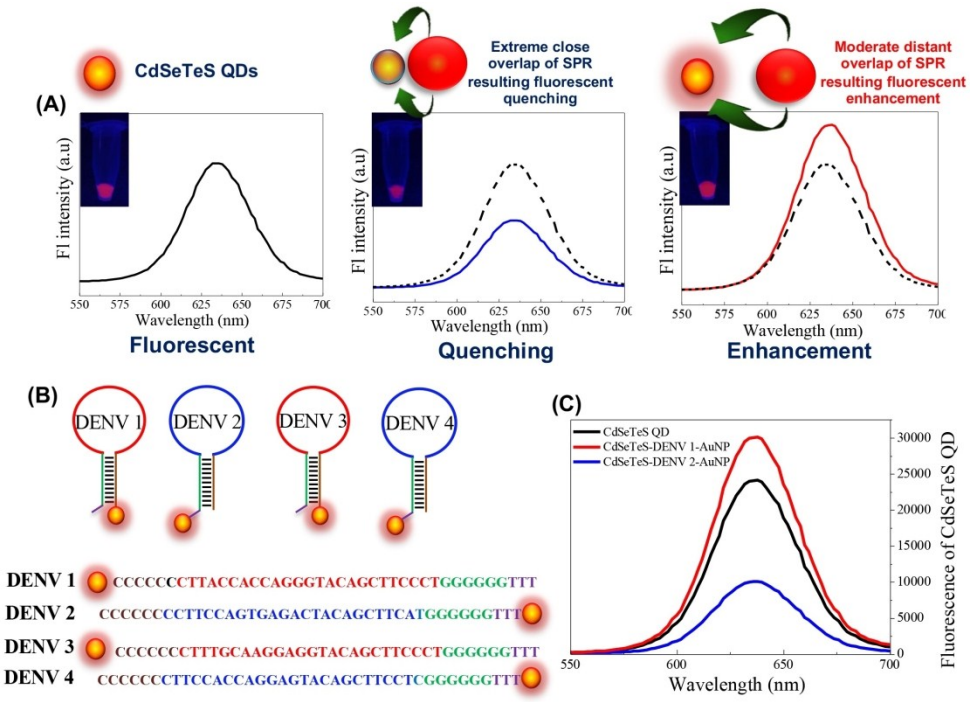

Fig. 4

190x133mm (300 x 300 DPI)

View Article Online
DOI: 10.1039/C9NA00763F

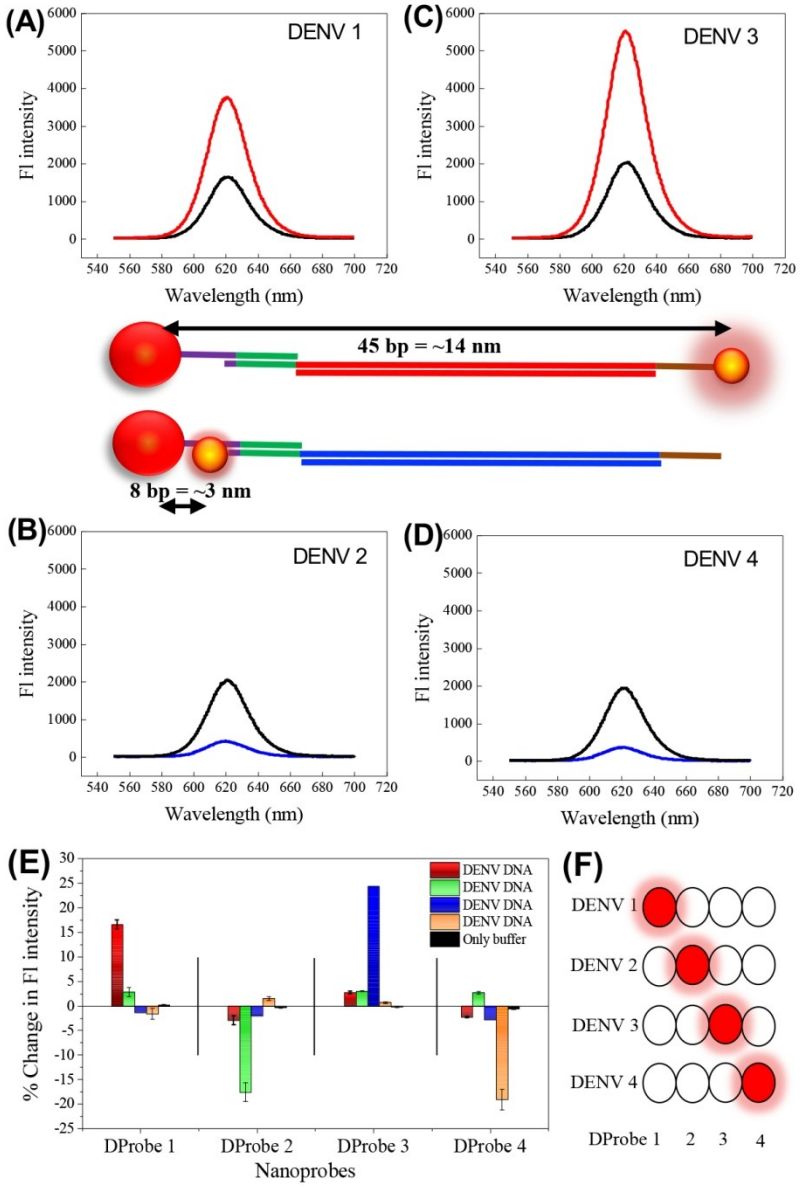

Fig. 5

View Article Online
DOI: 10.1039/C9NA00763F

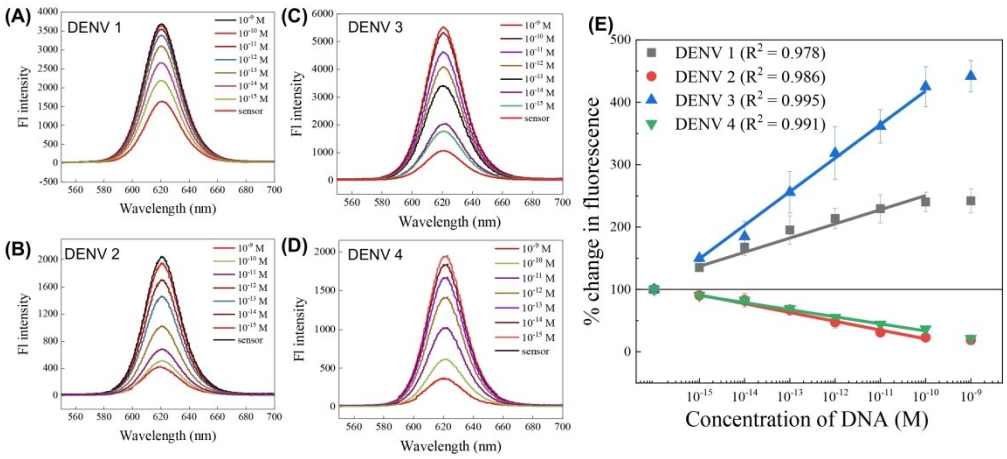

Fig. 6

254x116mm (300 x 300 DPI)

View Article Online
DOI: 10.1039/C9NA00763F

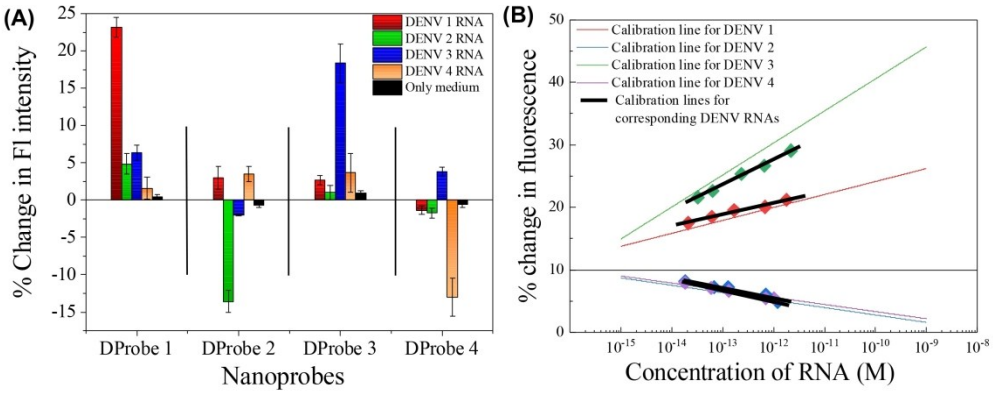

Fig. 7

249x98mm (300 x 300 DPI)